*Journal of Advanced Ceramics*
2018, **7**(4): 336–342
https://doi.org/10.1007/s40145-018-0283-3
ISSN 2226-4108
CN 10-1154/TQ

**Research Article**

# Study on water corrosion behavior of $ZrSiO_4$ materials

Ling LIU[a,b], Wei ZHENG[a,b], Zhuang MA[a,b,*], Yanbo LIU[a,b,*]

[a]*School of Materials Science and Engineering, Beijing Institute of Technology, Beijing 100081, China*
[b]*National Key Laboratory of Science and Technology on Materials under Shock and Impact, Beijing 100081, China*

Received: March 14, 2018; Revised: May 7, 2018; Accepted: May 9, 2018


**Abstract:** $ZrSiO_4$ bulk was prepared by pressureless sintering process and $ZrSiO_4$ coating was deposited on the $SiC_f$/SiC substrate using air plasma method. The microstructures of $ZrSiO_4$ bulk and $ZrSiO_4$ coating are both dense. A preliminary study of a water vapor corrosion test for $ZrSiO_4$ bulk and $ZrSiO_4$ coating was performed under the conditions of $1.013\times10^5$ Pa, 90%$H_2O$/10%$O_2$, 1300 ℃, and low gas velocity. Results show that some pores appear on the surface of the $ZrSiO_4$ bulk. The main crystal phase is $ZrO_2$ and the weight loss of $ZrSiO_4$ bulk is only 0.236 mg/cm$^2$ after corrosion. The $ZrSiO_4$ coating peels off from the substrate after 109 h. The number and intensity of diffraction peaks of $ZrO_2$ in the coating increase, and the major crystal phase of the coating is still $ZrSiO_4$. A porous microstructure accompanied with cracks is observed on the surface of $ZrSiO_4$ coating after corrosion.

**Keywords:** $ZrSiO_4$; $SiC_f$/SiC substrate; environmental barrier coating (EBC); water vapor corrosion behavior

## 1 Introduction

The efficiency and core power of gas turbine engines used in aircraft are directly related to the turbine inlet temperature, where a higher operation temperature provides better turbine performance [1]. While the nickel-based superalloys (1100 ℃) cannot endure higher temperatures (up to 1316 ℃) due to the low melting points of the metallic components [2], silicon carbide fiber/silicon carbide ($SiC_f$/SiC) substrate has been widely considered as the most promising component of next-generation aircraft gas turbine engines [3,4]. The protection of the silica layer makes it possible to use $SiC_f$/SiC in dry air. However, when exposed to combustion environment containing water vapor, $SiC_f$/SiC is oxidized and is subsequently corroded to form gaseous silica hydroxide, causing weight loss and failure of ceramic components [5].

In order to successfully apply silicon-based ceramics in high temperature combustion environment (up to 1316 ℃), an environmental barrier coating (EBC) was developed to protect it from water vapor corrosion and to improve the temperature durability of hot section in combustion environment [3,6]. The EBC materials must have chemical stability at high temperature, low thermal conductivity, and a coefficient of thermal expansion (CTE) that matches the substrate to avoid cracking between the layers [4,7,8]. Therefore, many materials were examined as candidates for EBC, which are expected to prevent oxidation degradation of

* Corresponding authors.
E-mail: Z. Ma, hstrong929@bit.edu.cn;
Y. Liu, boobbyy@163.com

silicon-based ceramics [9,10]. And in order to improve the comprehensive performance of environmental barrier coating, the low CTE materials such as rare earth silicate, $RESi_2O_5$, and $RE_2Si_2O_7$ coatings (RE = rare earth elements, including Sc, Yb, Er, and Lu) have been developed [6,11,12].

Even though rare earth silicates exhibit excellent water vapor resistance, the Si–O bonds in silicates react with water vapor to cause the material recession [6,13–15]. As a result, new EBC materials have been developed in recent years. Among the low thermal expansion silicate compounds, $ZrSiO_4$ is a potential material because its thermal stability is more preferable and its CTE ($4.43\times10^{-6}$ (℃)$^{-1}$) is almost the same as that of silicon-based ceramics (($(4–5)\times10^{-6}$ (℃)$^{-1}$) [16,17]. In the case of silicon nitride with $ZrSiO_4$, the $ZrSiO_4$ layer and the substrate remain adherent during the test, and $ZrSiO_4$ sample has a low corrosion rate [18], which makes $ZrSiO_4$ have potential applications in the field of EBCs. But there are currently few reports on $ZrSiO_4$ as a water corrosion coating. In this paper, the water vapor corrosion behavior of $ZrSiO_4$ ceramic and $ZrSiO_4$ coating at 1300 ℃ was investigated and the recession mechanism was revealed.

## 2 Experimental

### 2. 1 Preparation of $ZrSiO_4$ bulk and $ZrSiO_4$ coating

The main raw material used in this work was $ZrSiO_4$ powders (≥ 99.9%, 1–3 μm, Huizhou Ruier Chemicals Technology Co., Ltd., Guangdong, China). The $ZrSiO_4$ bulk was prepared by pressureless sintering process at 1400 ℃, sintered twice for 5 h. And the as-sintered density was measured according to the Archimedes principle. The $SiC_f$/SiC composite materials with the size of 17 mm × 15 mm × 3 mm were provided by Research Center of Composite Materials. The coated sample was composed of the $SiC_f$/SiC substrate and the $ZrSiO_4$ layer. The spray powders with high flowability were obtained by spray drying granulation method. The slurry for spray drying which was composed of $ZrSiO_4$ powders, polyvinyl alcohol (PVA, 0.5 wt%), and deionized water was ball milled for 2 h. Ball milling is used to crush the powders and reduce the agglomeration phenomenon between the powders. The solid content of slurry was 30 wt%. The powders were obtained by spray granulation and calcination at 1400 ℃. The powders with the size in the range of 30–65 μm were collected as the thermal spraying feedstock. The substrates were grit-blasted to gain rough surface which can increase the bonding strength. Then the sprayed powders were deposited on the substrate with the rough surface by air plasma spraying process to obtain the $ZrSiO_4$ coating (about 120 μm in thickness). The $ZrSiO_4$ coating was decomposed after the air plasma spraying, thus the sample was subjected to a heat-retaining treatment in Ar at 1400 ℃ for 2 h after air plasma spraying according to the reference [19]. The spray parameters are shown in Table 1.

### 2. 2 Water oxygen corrosion test

The schematic diagram of water vapor corrosion test equipment is shown in Fig. 1. The test conditions were as follows: 90%$H_2O$/10%$O_2$ gas flow rate at 0.17 cm/s, $1.013\times10^5$ Pa, 1300 ℃. Gas mixture was generated by a tube furnace (GSL-1600X, Hefei Kejing Material Technology Co., Ltd.) and a gas generator (LVD-F1, Hefei Kejing Material Technology Co., Ltd.). By setting the known oxygen flow and controlling the flow of water vapor at a flow ratio of 9:1, the facility could produce 90%$O_2$ and 10%$H_2O$. The flow rate was calculated by summing the flow of oxygen and water vapor, and then dividing by the cross-sectional area of the furnace tube. Tube furnaces were vacuumed prior to the experiment. The exposure time was 14 h and the time interval was 10 h. The $ZrSiO_4$ bulk and $ZrSiO_4$ coating were placed on the alumina crucible. And the samples were slowly taken out from the furnace tube at regular intervals to accurately record the weight change to detect changes in the structure and phase of the samples. The $ZrSiO_4$ bulk and the $ZrSiO_4$-coated $SiC_f$/SiC were exposed multiple times to avoid repeatability and uncertainty of the results, and the final results were averaged.

### 2. 3 Analysis and characterization

The weight change of the specimens was determined by the electronic balance (FA2044J, Yueping Science Instrument Co., Ltd, Shanghai, China). The surface morphology of $ZrSiO_4$ bulk and the surface and cross-section morphology of $ZrSiO_4$ coating were

**Table 1 Parameters used in the air plasma spraying**

| Arc current (A) | Primary Ar (SCFH) | Secondary He (SCFH) | Powder feed rate (rpm) | Ar carrier gas flow rate (SCFH) | Spray distance (mm) |
|---|---|---|---|---|---|
| 850 | 90 | 30 | 3.0 | 10 | 75 |

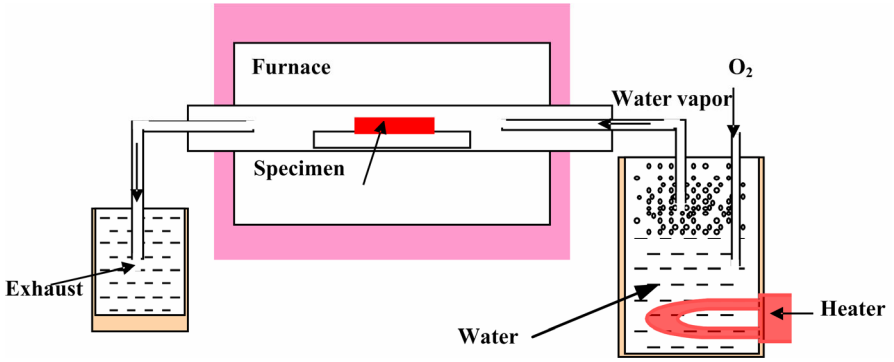


**Fig. 1** Schematic diagram of experimental equipment for water vapor corrosion.

characterized by scanning electron microscope (SEM, Philips S-4800, Hitachi Ltd., Yokohama, Japan); the phase compositions of $ZrSiO_4$ bulk and $ZrSiO_4$ coating were determined by X-ray diffractometer (XRD, RIGAKU D/Max-rB, Rigaku International Corp., Tokyo, Japan) with the scan rate of 4 (°)/min, and the composition of the $ZrSiO_4$ coating was analyzed by energy spectrum analyzer (EDS).

## 3 Results and discussion

### 3. 1 Water oxygen corrosion behavior of $ZrSiO_4$ bulk

The microstructure of the $ZrSiO_4$ ceramic bulk before and after corrosion is shown in Fig. 2. It can be seen that the surface morphology of the sample before corrosion is flat and dense, and the relative density of $ZrSiO_4$ bulk measured by Archimedes principle is above 98% (Fig. 2(a)). There are many pores and the grains grown after corrosion (Fig. 2(b)); the relative density of $ZrSiO_4$ bulk is 93.40% and the pores may be caused by volatilization of gases.

Figure 3 shows the phase composition of the $ZrSiO_4$ bulk before and after corrosion. Before the experiment, a small amount of $ZrO_2$ diffraction peaks exist in $ZrSiO_4$ bulk (Fig. 3(a)). After corrosion, the intensity of the diffraction peaks of $ZrO_2$ increases. The main crystal phase is $ZrO_2$, and a small amount of $ZrSiO_4$ diffraction peaks exist in the bulk (Fig. 3(b)). The $ZrSiO_4$ phase decomposed into $SiO_2$ and $ZrO_2$ above 1500 ℃ [20], and the corrosion test was performed at 1300 ℃ that is much lower than 1500 ℃. Therefore, during the corrosion test, the $ZrO_2$ phase was generated by the reaction of $ZrSiO_4$ and $H_2O$ according to Eq. (1) rather than by thermal decomposition. The pores in Fig. 2(b) were caused by

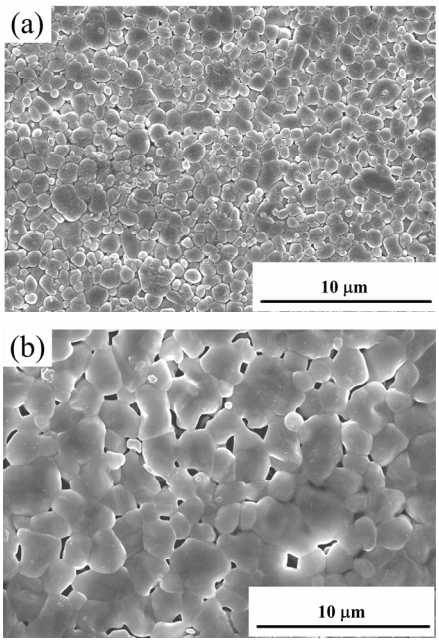


**Fig. 2** Microstructure of the $ZrSiO_4$ bulk (a) before and (b) after corrosion.

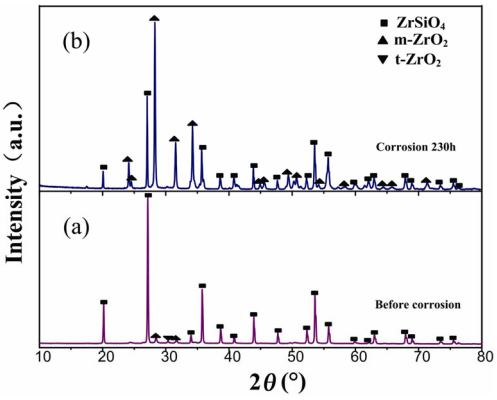


**Fig. 3** Phase composition of the $ZrSiO_4$ bulk (a) before and (b) after corrosion.

the volatilization of $Si(OH)_4$ gas produced in Eq. (1), and the grain growth was due to long-term exposure to

1300 ℃.

$$ZrSiO_4(s) + 2H_2O(g) \rightarrow ZrO_2(s) + Si(OH)_4(g) \quad (1)$$

The weight change curve of $ZrSiO_4$ ceramic bulk is shown in Fig. 4. With the increase of corrosion time, the mass change of the bulk is very small. And the weight loss of the sample is only 0.236 mg/cm$^2$ after 230 h, which is due to the volatilization of $Si(OH)_4$ gas during the corrosion experiment.

### 3. 2 Water oxygen corrosion behavior of $ZrSiO_4$ coating

The weight change curve of $ZrSiO_4$ coating is shown in Fig. 5 under the condition of corrosion at 1300 ℃. It can be seen that the mass loss rate per unit area of the sample protected by $ZrSiO_4$ coating is small, and the sample has been in steady gain state in the early corrosion test. After 109 h, the coating peels off.

From the cross-sectional morphology of $ZrSiO_4$ coating in Fig. 6, it can be seen that before corrosion the coating is uniform and dense. In addition, there are no penetrating cracks and pores throughout the coating area, and no obvious defects are present at the interface between the coating and the substrate. Therefore, the coating structure does not form oxygen and water vapor channels, and it can isolate the intrusion of oxygen and water vapor (Fig. 6(a)). After the corrosion, it appears from the SEM results (Fig. 6(b)) that the crack occurs in the $ZrSiO_4$ coating near the underlying $SiC_f$/SiC, but not at the interface. The EDS results are also consistent with formation of a thermally grown $SiO_2$ layer.

Figure 7 shows the surface morphology of $ZrSiO_4$ coating before and after corrosion. The surface of the coating is relatively flat and most of the powder particles are completely melted and spread out, showing a flat topography (Fig. 7(a)) before the corrosion experiment. After 109 h of water vapor corrosion test, a porous microstructure accompanied with some cracks (Figs. 7(b) and 7(c)) is observed on the surface of $ZrSiO_4$ coating.

Table 2 shows the ratio of Si and Zr in the $ZrSiO_4$ coating at different corrosion time. It can be seen that the ratio of Si and Zr decreases first and then increases. It can be seen from Fig. 8 that the major crystalline

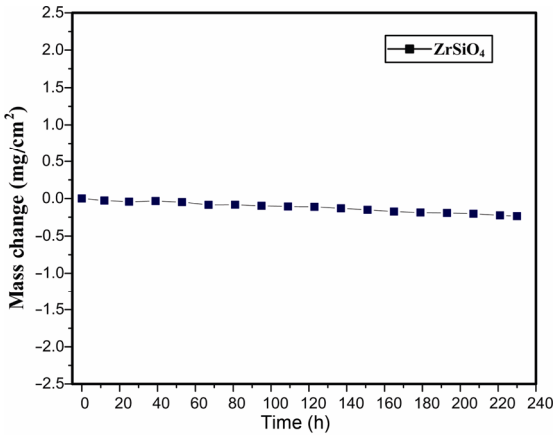


**Fig. 4** Weight loss of $ZrSiO_4$ bulk in 90%$H_2O$/10%$O_2$ at 1300 ℃.

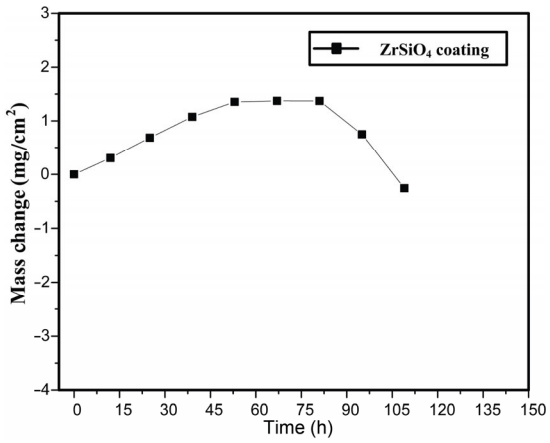


**Fig. 5** Weight loss of $ZrSiO_4$ coating in 90%$H_2O$/10%$O_2$ at 1300 ℃.

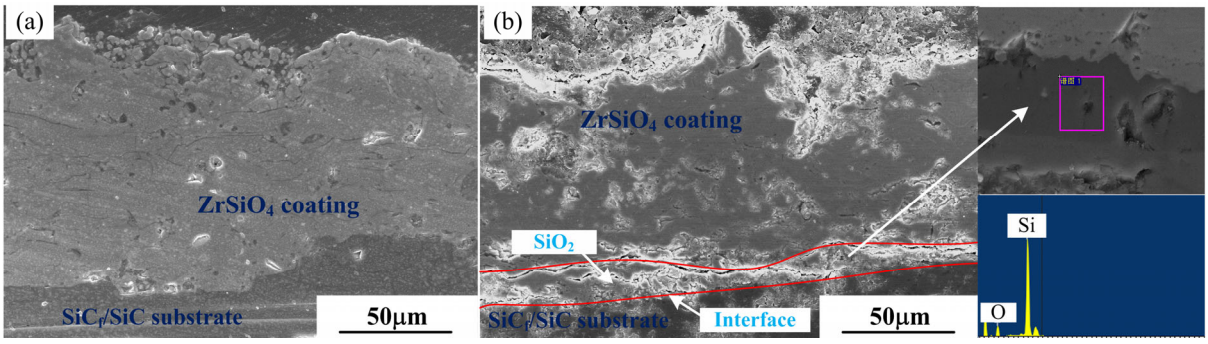


**Fig. 6** Morphology of the section of the $ZrSiO_4$ coating (a) before and (b) after corrosion.

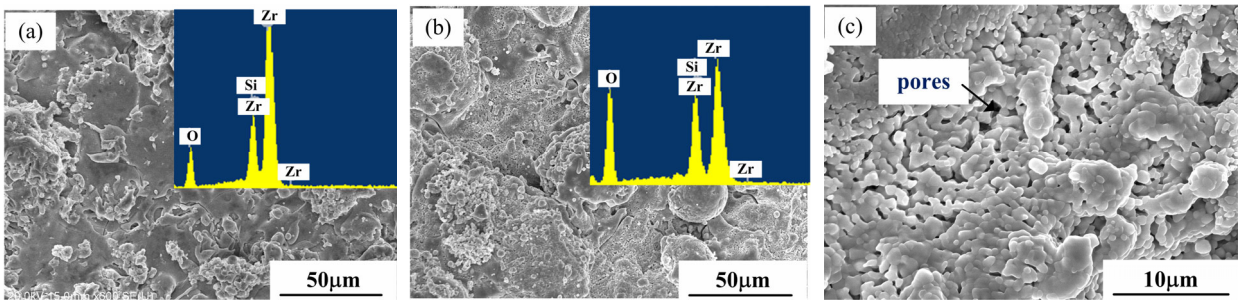


**Fig. 7** Surface morphology of the $ZrSiO_4$ coating (a) before and (b) after corrosion and (c) magnified of (b).

**Table 2 Ratio of Si and Zr in $ZrSiO_4$ coating at different corrosion time**

| | Before corrosion | Corrosion 85 h | Corrosion 109 h |
|---|---|---|---|
| Si/Zr | 0.90 | 0.35 | 0.44 |

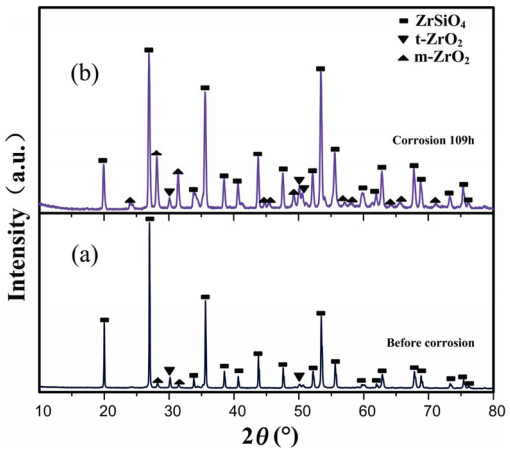


**Fig. 8** Phase change of $ZrSiO_4$ coating (a) before and (b) after corrosion.

phase of the coating is $ZrSiO_4$, and a small amount of $ZrO_2$ is present before corrosion (Fig. 8(a)). After 109 h of corrosion, the number and intensity of diffraction peaks of $ZrO_2$ in the coating increase, but $ZrSiO_4$ is the major crystal phase of the coating (Fig. 8 (b)).

### 3.3 Recession mechanism of $ZrSiO_4$ coating

A small amount of $SiO_2$ was volatilized during the spraying process, thus a small amount of $ZrO_2$ is present in the $ZrSiO_4$ coating after the heat-retaining treatment (Fig. 8(a)). From the recession mechanism of $ZrSiO_4$ bulk, the phase change, and the decrease of Si content in the coating after corrosion, it can be determined that $ZrSiO_4$ reacted with $H_2O$ to form $ZrO_2$ and $Si(OH)_4$ gas during the experiment (Fig. 9(a)). Thus the porous microstructure in Fig. 7(c) is due to the volatilization of $Si(OH)_4$ gas, and therefore the surface is depleted in $SiO_2$ with a relative enrichment in $ZrO_2$ (The EDS map of Figs. 7(a) and 7(b)). The corrosion of $ZrSiO_4$ under water vapor conditions is a preferential corrosion in grain boundary of $ZrSiO_4$. The increase in porosity of $ZrSiO_4$ after the corrosion test is in good agreement with a past result (pressurized steam test of $ZrSiO_4$ coating) [21]. In addition, the thermal expansion coefficient of $ZrO_2$ ($10.5\times10^{-6}$ $(K)^{-1}$) produced by reaction (1) is very different from that of $ZrSiO_4$ and the $SiC_f$/SiC substrate, which results in a certain residual stress during the cooling process. In the long-term water oxygen environment at high temperature and cooling conditions, the internal residual stress increases, leading to internal cracks in the coating (Fig. 9(b)). The pores and cracks in the

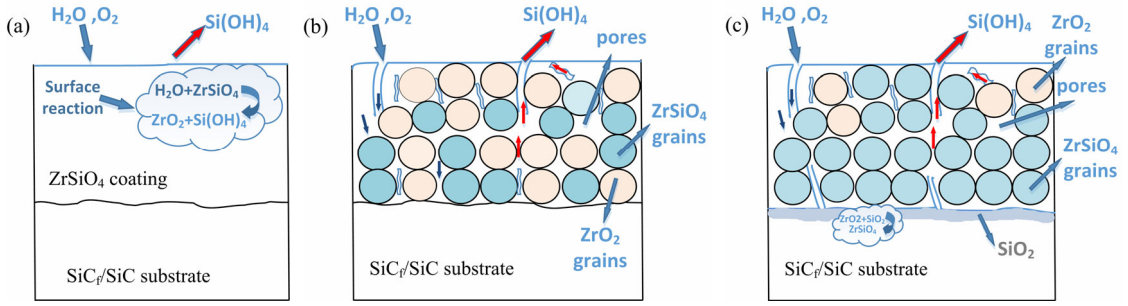


**Fig. 9** Corrosion recession mechanism of $ZrSiO_4$ coating in water vapor corrosion environment: (a) initial stage of volatilization, (b) pores and a large amount of $ZrO_2$ grains appear in the surface layer, and (c) late in the corrosion process.

coating form the $O_2$ and $H_2O$ channels. $O_2$ and the substrate react to produce $SiO_2$, resulting in an increase in the weight of the sample. Volatilization of $Si(OH)_4$ gas generated by the reaction of $SiO_2$ with $H_2O$ and the reaction of $ZrSiO_4$ with $H_2O$, result in the sample weight decrease (Fig. 5). But $ZrSiO_4$ is the main crystal phase in the coating after corrosion, indicating that the $ZrO_2$ produced by reaction (1) reacts with the $SiO_2$ formed by the oxidation of the substrate to form a certain amount of $ZrSiO_4$.

After 109 h, due to the volatilization of $Si(OH)_4$ gas, the presence of high thermal expansion coefficient of $ZrO_2$, and the oxidation of the substrate, there are many defects in the coating and the coating separates from the substrate, resulting in premature coating from the substrate peeling off.

## 4 Conclusions

In this paper, the dense $ZrSiO_4$ ceramic bulk was prepared by pressureless sintering process, and the dense $ZrSiO_4$ layer was successfully deposited on $SiC_f$/SiC substrate using air plasma spray method. The water vapor corrosion behavior of $ZrSiO_4$ bulk and $ZrSiO_4$ coating at 1300 ℃ was investigated. After the corrosion, the weight loss of the $ZrSiO_4$ bulk is only 0.236 mg/cm$^2$. A porous microstructure is observed on the surface of the $ZrSiO_4$ coating due to the volatilization of $Si(OH)_4$ gas. The $ZrSiO_4$ coating peels off after 109 h and some cracks appear on the surface of the coating. During the corrosion test, the $ZrO_2$ produced by the reaction of $ZrSiO_4$ and $H_2O$ in the coating reacts with the $SiO_2$ formed by the oxidation of the substrate, thus $ZrSiO_4$ is the main crystal phase of the coating. The durability is a key factor for EBC materials, but such $ZrSiO_4$ coating could not withstand more than 200 h at 1300 ℃ in combustion environment. Therefore, $ZrSiO_4$ materials need to be improved in terms of EBC materials.

### Acknowledgements

This work was supported by the National Natural Science Foundation of China under Grant No. 51772027.

### References

[1] Perepezko JH. The hotter the engine, the better. *Science* 2009, **326**: 1068–1069.

[2] Lin F, Jiang XL. Research development of thermal barrier coatings. *Journal of Functional Materials* 2003, **34**: 254–257. (in Chinese)

[3] Lee KN, Fox DS, Eldridge JI, *et al.* Upper temperature limit of environmental barrier coatings based on mullite and BSAS. *J Am Ceram Soc* 2003, **86**: 1299–1306.

[4] Richards BT, Wadley HNG. Plasma spray deposition of tri-layer environmental barrier coatings. *J Eur Ceram Soc* 2014, **34**: 3069–3083.

[5] Opila EJ. Oxidation and volatilization of silica formers in water vapor. *J Am Ceram Soc* 2003, **86**: 1238–1248.

[6] Lee KN, Fox DS, Bansal NP. Rare earth silicate environmental barrier coatings for SiC/SiC composites and $Si_3N_4$ ceramics. *J Eur Ceram Soc* 2005, **25**: 1705–1715.

[7] Cao XQ, Vassen R, Stoever D. Ceramic materials for thermal barrier coatings. *J Eur Ceram Soc* 2004, **24**: 1–10.

[8] Cernuschi F, Bianchi P, Leoni M, *et al.* Thermal diffusivity/microstructure relationship in Y-PSZ thermal barrier coatings. *J Therm Spray Tech* 1999, **8**: 102–109.

[9] Lee KN, Miller RA. Oxidation behavior of mullite-coated SiC and SiC/SiC composites under thermal cycling between room temperature and 1200°–1400°C. *J Am Ceram Soc* 1996, **79**: 620–626.

[10] Lee KN. Current status of environmental barrier coating for Si-based ceramics. *Surf Coat Technol* 2000, **133–134**: 1–7.

[11] Darthout É, Gitzhofer F. Thermal cycling and high-temperature corrosion tests of rare earth silicate environmental barrier coatings. *J Therm Spray Tech* 2017, **26**: 1–15.

[12] Richards BT, Sehr S, Franqueville FD, *et al.* Fracture mechanisms of ytterbium monosilicate environmental barrier coatings during cyclic thermal exposure. *Acta Mater* 2016, **103**: 448–460.

[13] Hong Z, Cheng L, Zhang L, *et al.* Water-vapor corrosion behavior of scandium silicates at 1400℃. *J Am Ceram Soc* 2009, **92**: 193–196.

[14] Nasiri NA, Patra N, Horlait D, *et al.* Thermal properties of rare-earth monosilicates for EBC on Si-based ceramic composites. *J Am Ceram Soc* 2016, **99**: 589–596.

[15] Fernández-Carrión AJ, Allix M, Becerro AI. Thermal expansion of rare-earth pyrosilicates. *J Am Ceram Soc* 2013, **96**: 2298–2305.

[16] Klemm H. Silicon nitride for high-temperature applications. *J Am Ceram Soc* 2010, **93**: 1501–1522.

[17] Ueno S, Ohji T, Lin HT. Corrosion and recession behavior of zircon in water vapor environment at high temperature.

*Corros Sci* 2007, **49**: 1162–1171.

[18] Ueno S, Jayaseelan DD, Ohji T, *et al.* Corrosion and oxidation behavior of $ASiO_4$ (A=Ti, Zr and Hf) and silicon nitride with an $HfSiO_4$ environmental barrier coating. *J Ceram Process Res* 2005, **6**: 81–84.

[19] Qian YB, Zhang WG. Phase-transformation behavior of plasma-sprayed $ZrSiO_4$ coating materials. *Journal of the Chinese Ceramic Society* 2008, **36**: 1103–1108. (in Chinese)

[20] Anseau MR, Biloque JP, Fierens P. Some studies on the thermal solid state stability of zircon. *J Mater Sci* 1976, **11**: 578–582.

[21] Yeom H, Lockharta C, Mariani R, *et al.* Evaluation of steam corrosion and water quenching behavior of zirconium-silicide coated LWR fuel claddings. *J Nucl Mater* 2018, **499**: 256–267.